IRAMP
13(2), July 2022, pp. 79-86

ISSN: 2229-39-44

Cavity Ring-Down Spectroscopy of CH in a Microwave Plasma Discharge

LÁSZLÓ NEMES[1] AND CHRISTIAN G. PARIGGER[2]

[1]*Research Center for Natural Sciences,*
Institute for Materials and Environmental Chemistry,
1117 Budapest, Magyar tudosok korutja 2, Hungary; nemesl@chemres.hu
[2]*Physics and Astronomy Department, University of Tennessee,*
University of Tennessee Space Institute, Center for Laser Applications,
411 B.H. Goethert Parkway, Tullahoma, USA; cparigge@tennessee.edu

ABSTRACT: This work communicates cavity ring-down spectroscopy (CRDS) of methylidyne (CH) in a chemiluminescent plasma that is produced in a microwave cavity. Of interest are the rotational lines of the 0-0 vibrational transition for the A-X band and the 1-0 vibrational transition for the B-X band. The reported investigations originate from CH-radical research in 1996 that constituted the first case of applying CRDS to the CH radical. The report also includes recent analysis that shows excellent agreement of measured and computed data, and it communicates CH line strength data.

KEYWORDS: Molecular spectroscopy; Diatomic molecules; Cavity ring-down spectroscopy; Absorption spectroscopy; Methylidyne; Line strength data; Plasma physics; Astrophysics

1. INTRODUCTION

Cavity ring-down spectroscopy (CRDS) was introduced by O'Keefe and Deacon in 1988 [1] and has since been used to an increasing extent for the measurement of weak absorbers or minute amounts of substances in the gaseous phase. Thus overtone bands [2] and the Herzberg absorption system in molecular oxygen [3] have been analyzed this way. Jet-cooled metal clusters [4, 5] and trace gas components [6] were probed by CDRS. Additionally, CDRS has proved eminently applicable for chemical kinetic system analysis, e.g., see Refs. [7, 8], that often involve transient radicals. Free radicals such as oxymethyl (HCO) in hydrocarbon ames [9] or the methyl (CH3) radical [10] were studied by this technique. We have applied this method in the form of coherent CRDS [11] to the spectroscopic analysis of the mehylidyne (CH) radical.

This report communicates selected data records from investigations in 1996. Specically, the CH B-X transition has been subject research in subsequent years [12-14]. In addition, this report summarizes recent analysis that utilizes accurate line strength data for CH [15, 16], and provides the CH line strength data for the A-X and B-X transitions. The line strength files (LSFs) for CH can also be applied for analysis of emission spectra that may be collected in laser-induced breakdown spectroscopy [17, 18]. The work in this report may have applications in astrophysics [19-21], combustion studies [22] and diamond film chemical vapor deposition [23].

2. EXPERIMENTS AND COMPUTATIONS

A. Experiment Details

The CH radicals were generated by the oxydation of acetylene (C2H2) using excited oxygen atoms produces in an inductively coupled microwave plasma (200 W at 2.45 GHz) in oxygen gas bubbled through water. The discharge was initiated in argon employing a ow inlet a few centimeters from the cavity mirrors. The flow of argon suppressed etching of the coating of the reflective mirrors by the flow of radicals. The chemiluminescent reaction leading to the generation of CH in the CDRS cavity occurred upon mixing the wet oxygen and acetylene via a distributed set of inlet openings, while the cavity was continuously pumped by two Roots pumps of a total capacity of 500 m^3/hour. This source was previously described by Ubachs et al. [24] The total pressure of the reactive gas mixture (Ar, O_2, C_2H_2 and water vapor) was kept at 400 Pa (3 Torr), as this provided the optimum setting for the CRDS signals. The CDRS mirrors had reectivities of R_1 =0.993 and R_2 =0.997, in the 363-nm to 430-nm range.

B. Diatomic Spectra Computation Details

The computations of the A-X and B-X transitions of CH rely on establishment of accurate line strengths. For analysis of the measured CH transitions, two sets of line strength files are communicated as supplement to this work. The development of line strength data is discussed with specific details for the C_2 Swan bands, computation of laser-induced fluorescence- and absorption- spectra [15]. The computation of line strengths for diatomic molecules follows recently published procedures [16]. Several applications in the analysis of optical breakdown spectra are communicated [16-18], including data files and the two programs, i.e., Boltzmann equilibrium spectrum program (BESP) and Nelder-Mead temperature (NMT), for analysis of selected diatomic molecules [25].

Tables I and II communicate excerpts of the set of line strength data applicable for analysis of recorded CRDS data. These data files can be conveniently utilized with BESP and NMT, see Ref. [25]. For computation of emission spectra in the analysis of laser-plasma, only the wave number, upper term value, and line strengths are needed. For computation of emission spectra [18], MATLAB [26] source code[27] has been made available recently. However, for computation of absorption spectra, the lower term values are required. The collated CH data files in Tabs. I and II also show standard designations for diatomic molecules [28]: J' upper and J" lower total angular momentum quantum number (nuclear spin not included); P_{ij}, or Q_{ij}, or R_{ij}, line designation based on J', J'', $F_{J'}$, $F_{J''}$; v' upper and v'' lower vibrational quantum number; p' upper and p'' lower parity designations, the $\pm$ total parity eigenvalue is followed by the e/f parity; N' upper and N'' lower total orbital angular momentum quantum number; $F_{J'}$ upper and $F_{J''}$ lower term value computed from model Hamiltonian, cm^{-1}; $\tilde{\nu}$ vacuum wavenumber, $\tilde{\nu} = F_{J'} - F_{J''}$, cm^{-1}; $S_{J'J''}$ Hönl-London term, unitless; $S_{n'v'J'n''v''J''}$ line strength, stC^2 cm^2 (1stC = 3.356 x 10^{-10} C).

Table I. First two dozen of 1384 lines for the CH $A\,^2\Delta \leftrightarrow X\,^2\Pi$ line strength table.

J'	J''		v'	v''	p'	p''	N'	N''	$F_{J'}$	$F_{J''}$	$\tilde{\nu}$	$S_{J'J''}$	$S_{S_{n'v'J'n''v''J''}}$
1.5	2.5	P22	0	0	+f	-f	2	3	24663.5612	1569.6083	23093.9531	0.2013	0.8026
1.5	2.5	P21	0	0	+f	-f	2	2	24663.5612	1489.0759	23174.4844	0.1996	0.7973
1.5	2.5	P11	0	0	-e	+e	1	2	24663.5612	1489.2381	23174.3223	0.2004	0.8001
1.5	2.5	P12	0	0	-e	+e	1	3	24663.5612	1569.1156	23094.4453	0.2005	0.7986
1.5	1.5	Q21	0	0	+f	-e	2	1	24663.5612	1433.8288	23229.7324	0.7998	3.200
1.5	1.5	Q22	0	0	+f	-e	2	2	24663.5612	1482.8608	23180.7012	0.8038	3.211
1.5	1.5	Q12	0	0	-e	+f	1	2	24663.5612	1483.1056	23180.4551	0.8075	3.224
1.5	1.5	Q11	0	0	-e	+f	1	1	24663.5612	1433.8051	23229.7559	0.7963	3.184
1.5	0.5	R22	0	0	+f	-f	2	1	24663.5612	1416.0299	23247.5312	2.005	8.020
1.5	0.5	R11	0	0	-e	+e	1	0	24663.5612	1415.9191	23247.6426	2.005	8.021
2.5	3.5	P12	0	0	-f	+f	2	4	24661.8291	1683.5813	22978.2480	0.0070179	0.027893
2.5	3.5	P11	0	0	-f	+f	2	3	24661.8291	1573.3187	23088.5098	0.3709	1.478

2.5	3.5	P21	0	0	+e	-e	3	3	24750.4863	1573.6950	23176.7910	0.2022	0.8070
2.5	3.5	P22	0	0	+e	-e	3	4	24750.4863	1682.7661	23067.7207	0.5651	2.248
2.5	3.5	P22	0	0	-f	+f	3	4	24750.4863	1683.5813	23066.9043	0.5666	2.254
2.5	3.5	P21	0	0	-f	+f	3	3	24750.4863	1573.3187	23177.1680	0.2009	0.8017
2.5	3.5	P11	0	0	+e	-e	2	3	24661.8291	1573.6950	23088.1348	0.3707	1.478
2.5	3.5	P12	0	0	+e	-e	2	4	24661.8291	1682.7661	22979.0625	0.0072268	0.028723
2.5	2.5	Q11	0	0	-f	+e	2	2	24661.8291	1489.2381	23172.5918	1.738	6.944
2.5	2.5	Q12	0	0	-f	+e	2	3	24661.8291	1569.1156	23092.7129	0.1448	0.5773
2.5	2.5	Q22	0	0	+e	-f	3	3	24750.4863	1569.6083	23180.8789	2.093	8.354
2.5	2.5	Q21	0	0	+e	-f	3	2	24750.4863	1489.0759	23261.4102	0.4911	1.964
2.5	2.5	Q21	0	0	-f	+e	3	2	24750.4863	1489.2381	23261.2480	0.4952	1.980
2.5	2.5	Q22	0	0	-f	+e	3	3	24750.4863	1569.1156	23181.3711	2.089	8.335

Table II. First two dozen of 261 lines for the $\mathrm{CH}\ B\,^2\Sigma^- \leftrightarrow X\,^2\Pi$ line strength table with column headings (identical to the ones in Table I).

J'	J''		v'	v''	p'	p''	N'	N''	$F_{J'}$	$F_{J''}$	$\tilde{\nu}$	$S_{J'J''}$	$S_{n'v'J'n''v''J''}$
0.5	1.5	P11	0	0	-f	+f	0	1	27114.2564	1433.9116	25680.3457	2.498	0.2572
0.5	1.5	P12	0	0	-f	+f	0	2	27114.2564	1483.2126	25631.0430	0.1750	0.018018
0.5	1.5	P22	0	0	+e	-e	1	2	27139.5581	1482.9686	25656.5898	2.493	0.2567
0.5	1.5	P21	0	0	+e	-e	1	1	27139.5581	1433.9356	25705.6230	0.1802	0.018552
0.5	0.5	Q11	0	0	-f	+e	0	0	27114.2564	1416.0057	25698.2500	1.337	0.1376
0.5	0.5	Q21	0	0	+e	-f	1	0	27139.5581	1416.1159	25723.4414	1.337	0.1376
1.5	2.5	P11	0	0	+f	-f	1	2	27139.5166	1489.1826	25650.3340	3.508	0.3612
1.5	2.5	P12	0	0	+f	-f	1	3	27139.5166	1569.7157	25569.8008	0.1008	0.010374
1.5	2.5	P22	0	0	-e	+e	2	3	27190.0681	1569.2245	25620.8438	3.505	0.3609
1.5	2.5	P21	0	0	-e	+e	2	2	27190.0681	1489.3449	25700.7227	0.1032	0.010624
1.5	1.5	Q12	0	0	+f	-e	1	2	27139.5166	1482.9686	25656.5488	0.019638	0.0020218
1.5	1.5	Q11	0	0	+f	-e	1	1	27139.5166	1433.9356	25705.5801	3.723	0.3833
1.5	1.5	Q21	0	0	-e	+f	2	1	27190.0681	1433.9116	25756.1562	0.017592	0.0018112
1.5	1.5	Q22	0	0	-e	+f	2	2	27190.0681	1483.2126	25706.8555	3.725	0.3835
1.5	0.5	R11	0	0	+f	-f	1	0	27139.5166	1416.1159	25723.4004	0.6683	0.068806
1.5	0.5	R21	0	0	-e	+e	2	0	27190.0681	1416.0057	25774.0625	0.6683	0.068803
2.5	3.5	P11	0	0	-f	+f	2	3	27189.9989	1573.4256	25616.5742	4.511	0.4645

2.5	3.5	P12	0	0	-f	+f	2	4	27189.9989	1683.6892	25506.3105	0.070992	0.0073091
2.5	3.5	P22	0	0	+e	-e	3	4	27265.6964	1682.8762	25582.8203	4.510	0.4643
2.5	3.5	P21	0	0	+e	-e	3	3	27265.6964	1573.8017	25691.8945	0.072257	0.0074393
2.5	2.5	Q11	0	0	-f	+e	2	2	27189.9989	1489.3449	25700.6543	5.838	0.6010
2.5	2.5	Q22	0	0	+e	-f	3	3	27265.6964	1569.7157	25695.9805	5.838	0.6011
2.5	1.5	R11	0	0	-f	+f	2	1	27189.9989	1433.9116	25756.0879	1.494	0.1538
2.5	1.5	R12	0	0	-f	+f	2	2	27189.9989	1483.2126	25706.7871	0.1099	0.011316

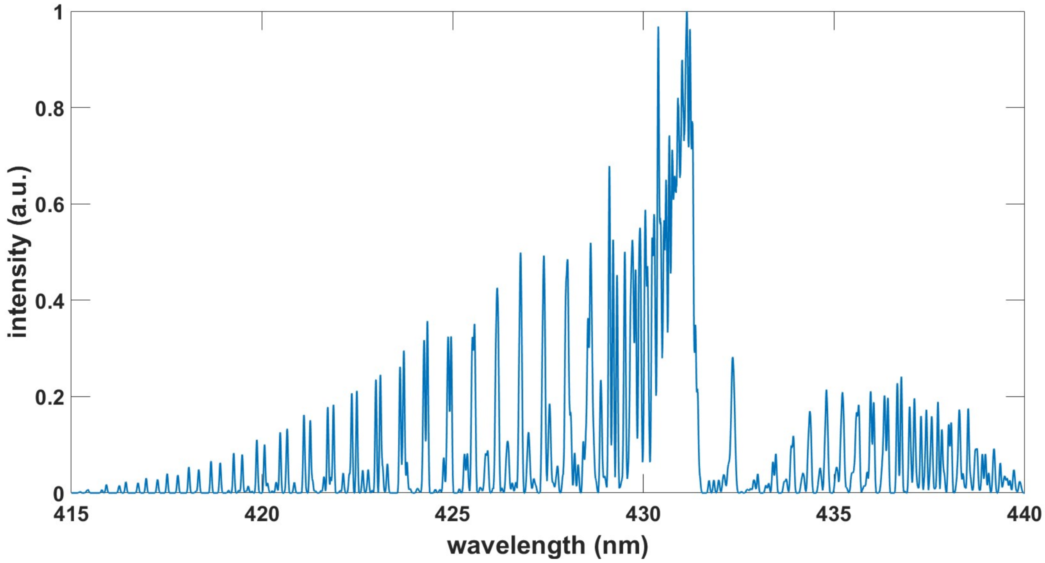

FIG. 1. Computed CH A-X spectrum, $\Delta \mathrm{v} = 0,\ \delta\lambda$ = 0.05 nm, T = 3.0 kK.

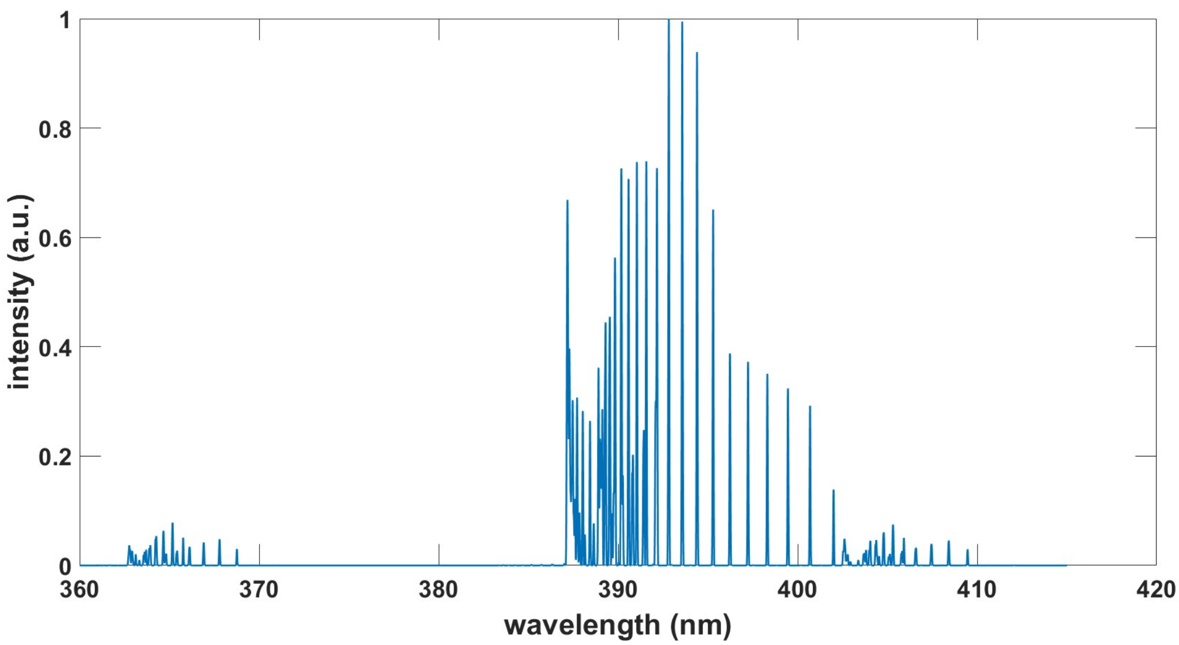

FIG. 2. Computed CH B-X spectrum, $\Delta \mathrm{v} = 0, +1,\ \delta\lambda$ = 0.05 nm, T = 3.0 kK.

III. RESULTS AND DISCUSSION

An overview plasma emission spectrum for CH A-X illustrates the wavelength range of the available line strength data. Figure 1 shows $\Delta v = 0$ transitions for v' = v" = 0, 1, 2. An instrument resolution, $\delta\lambda$, of $\delta\lambda$ = 0:05 nm is selected, and the equilibrium temperature, T, is set to 3.0 kK. Fig. 2 displays computed CH B-X spectra for v = 0; +1 transition, i.e., v' = v = 0, 1, and v' = 1 to v" = 0.

For cavity ring-down experiments, a Continuum model-TDL60 Nd:YAG-pumped dye laser was employed. The A-X transition access was accomplished with Coumarin 120 dye

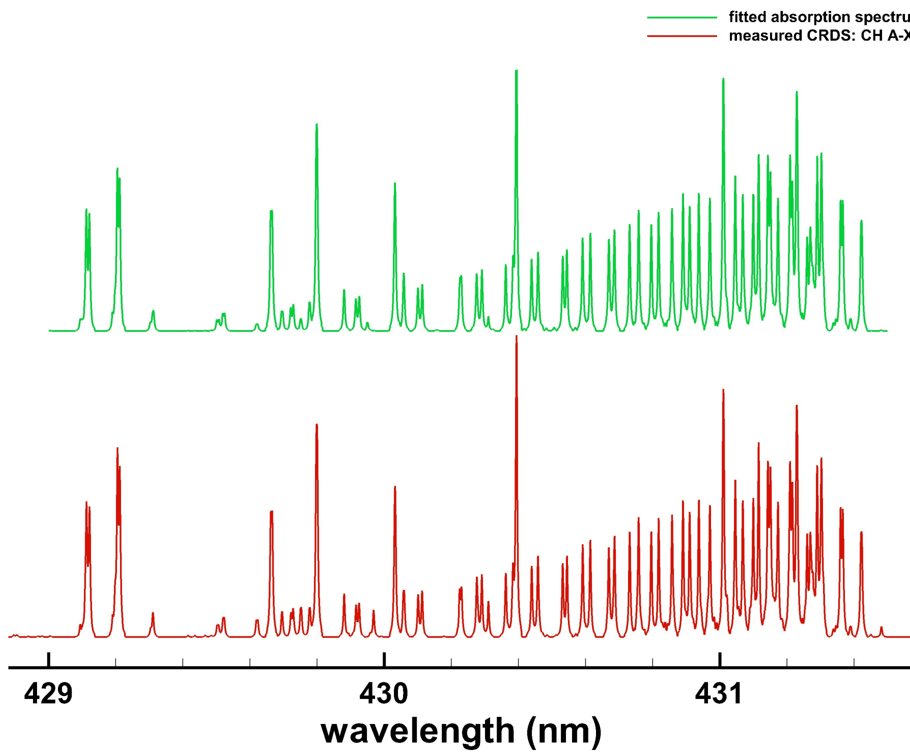

FIG. 3. Comparison of measured (bottom) and fitted (top) CH A-X spectra, $\delta\lambda$ = 0.005 nm, T = 1.47 kK.

that shows a gain maximum of 440 nm. The B-X transition was reached by frequency doubling the output using Styryl 7 dye that shows a gain maximum at 720 nm, or frequency doubled at 360 nm. The available output power ranged from 5 to 15 mJ per pulse, but it was attenuated with diaphragms for CRDS. Overview spectra were initially observed in emission using a low resolution Jobin-Yvon grating spectrometer. Methylidyne A-X bands were noticed near 430 nm that were stronger than the B-X bands near 390 nm, see Figures 1 and 2. In addition, C_2 Swan bands were observed near 470 nm, 520 nm, and 560 nm, e.g., see Ref. [25]. Figure 3 illustrates comparison of measured and fitted absorption spectra.

Figure 4 displays CRDS data of normalized absorption in the wavenumber range of 23160 cm^{-1} (431.779 nm) to 23320 cm^{-1} (428.816 nm). For completeness, Fig. 5 illustrates computed emission spectra in the same vacuum wavenumber range as for Fig. 4. As expected, there are subtle differences for comparisons of absorption spectra, see Fig. 3, or for comparison of CRDS data (Fig. 4) with spectra (Fig. 5) that are seen in emission from plasma.

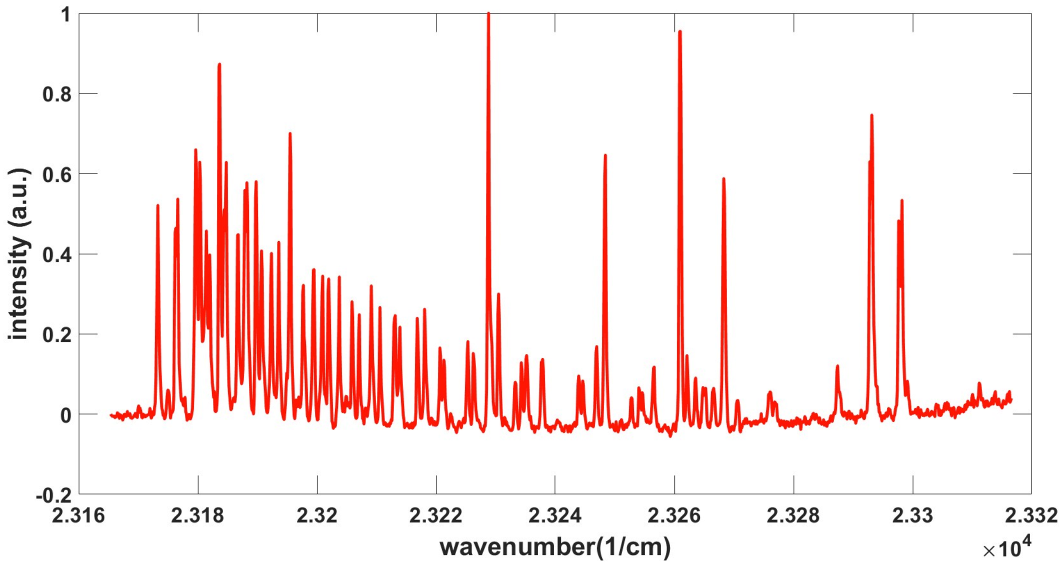

FIG. 4. Recorded CH A-X spectrum using CRDS.

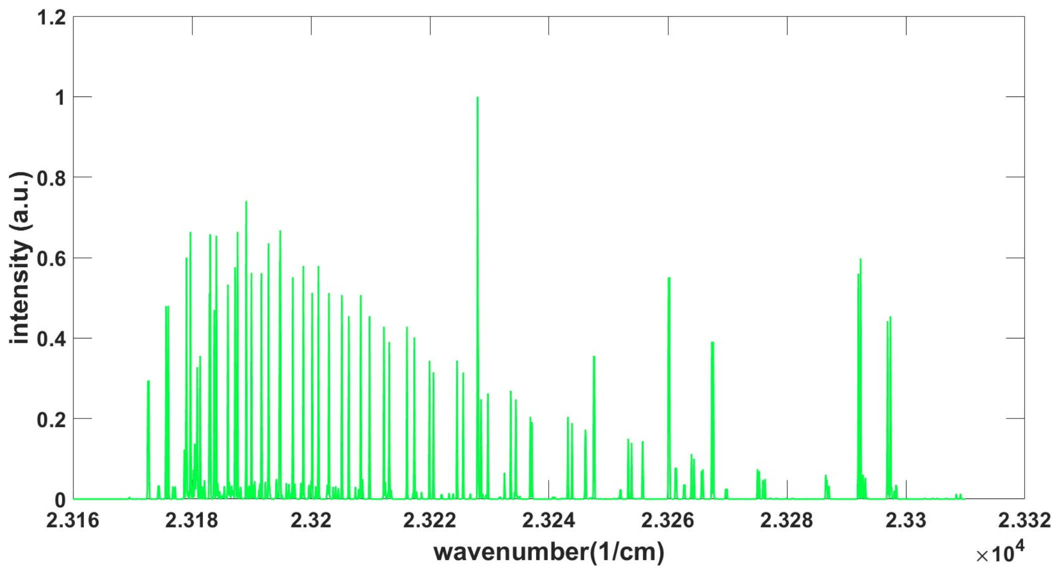

FIG. 5. Computed CH A-X emission spectrum, $\delta\tilde{\nu}$ = 0.1 cm^{-1}, T = 1.5 kK.

Figure 6 displays a recorded B-X CH spectrum, and Fig. 7 shows an emission spectrum for the same vacuum wavenumber range of 27400 cm^{-1} (364.964 nm) to 27470 cm^{-1} (364.033 nm).

IV. CONCLUSIONS

This work communicates a convincing comparison of recorded cavity ring-down spectra and of computed CH A-X absorption spectra using line strength data. Higher resolution for

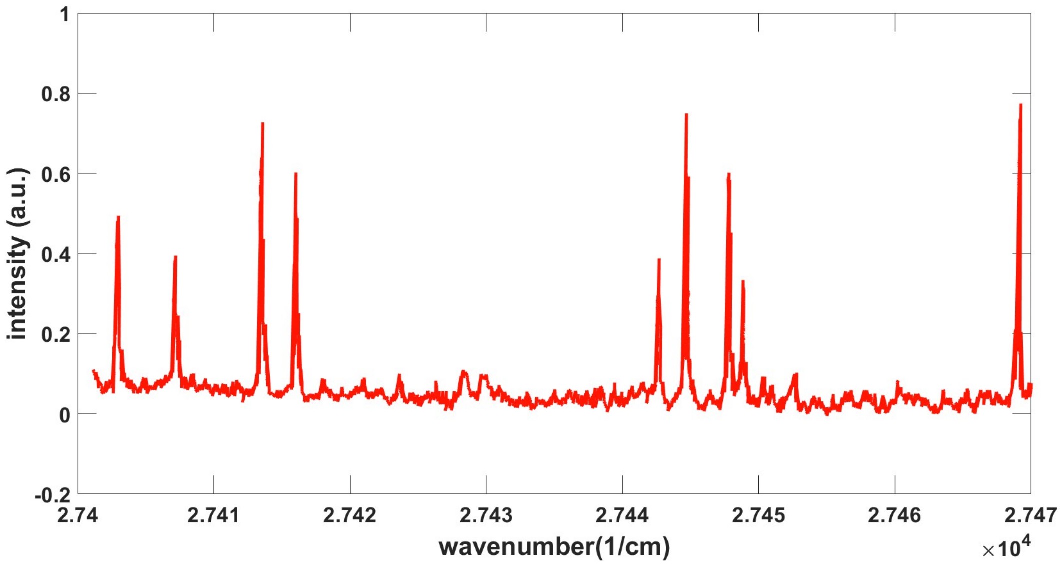

FIG. 6. Recorded CH B-X spectrum using CRDS.

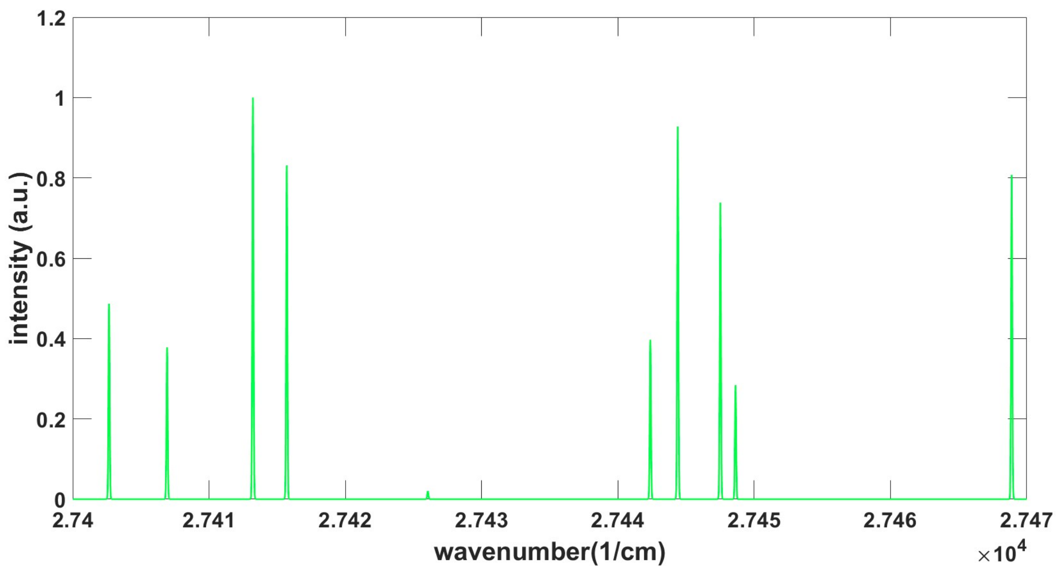

FIG. 7. Computed CH B-X emission spectrum, $\delta\tilde{\nu}$ = 0:1 cm^{-1}, T = 1.5 kK.

the investigated CH B-X transition than for the CH A-X transition also confirms reasonable accuracy of measured and computed line positions. Emission spectra of CH A-X and BX were observed but focus of this work was the application of CRDS for the CH radical. However, the provided line strength data are expected to be useful in emission spectroscopy of plasma that contains hydrocarbons.

ACKNOWLEDGMENTS

CGP acknowledges support in part by the State of Tennessee funded Center for Laser Applications at the University of Tennessee Space Institute. LN acknowledges a short term visiting scientist support from the Nederlandse Organistie voor Wetenschappelijk (NWO), as well as support from the Hungarian Research Fund (OTK #3079) for computational equipment in Hungary during the initial research analysis in 1996. Last but not least, LN and CGP acknowledge the consent of Professor Hans J.J. ter Meulen (University of Nijmegen, The Netherlands) to publishing the so far unpublished material and CRDS data.

References

[1] O'Keefe, A.; Deacon, D.A.G. Rev. Sci. Instrum. 59, 1988, 2544.

[2] Romanini, D.; Lehmann, K.K. J. Chem. Phys 1993, 99, 1993, 6287.

[3] Huestis, D.L.; Copeland, R.A.; Knutsen, K.; Slanger, T.G.; Jongma, R.T.; Boogaarts, M.G.H.; Meijer, G. Can. J. Phys. 72, 1994, 1109.

[4] Scherer, J.J.; Paul, J.B.; Collier, C.P.; Saykally, R.J. Chem. Phys. Lett. 102, 1995, 5190.

[5] O'Keefe, A.; Scherer, J.J.; Cooksy, A.L.; Sheeks, R.; Heath, J.; Saykally, R.J. Chem. Phys. Lett. 172, 1990, 214.

[6] Jongma, R.T.; Boogaarts, M.G.H.; Holleman, I.; Meijer, G. Rev. Sci. Instrum. 66, 1995, 2821.

[7] Yu, T.; Lin, M.C. J. Am. Chem. Soc. 115, 1993, 4371.

[8] Yu, T.; Lin, M.C. J. Phys. Chem. 98, 1994, 9697.

[9] Cheskis, S. J. Chem. Phys. 102, 1995, 1851.

[10] Zalicki, P.; Ma, Y.; Zare, R.N.; Wahl, E.H.; Dadamino, J.R.; Owano, T.G.; Kruger, C.H. Chem. Phys. Lett. 234, 1995, 269.

[11] Meijer, G.; Boogaarts, M.G.H.; Jongma, R.T.; Parker, D.H.; Wodtke, A.M. Chem. Phys. Lett. 217, 1994, 112.

[12] Wang, C.-C.; Nemes, L.; Lin, K.-C. Chem. Phys. Lett. 245, 1995, 585.

[13] Nemes, L.; Szalay, P.G. Models Chem. 136, 1999, 205.

[14] Szalay, P.G.; Nemes, L. Molec. Phys. 96, 1999, 359.

[15] Hornkohl, J.O.; Nemes, L; Parigger, C.G.; Spectroscopy of Carbon Containing Diatomic Molecules. In Spectroscopy, Dynamics and Molecular Theory of Carbon Plasmas and Vapors: Advances in the Understanding of the Most Complex High-Temperature Elemental System; Nemes, L., Irle, S., Eds.; World Scientic: Singapore, SG, 2011; Chap. 4, pp. 113-165.

[16] Parigger, C.G.; Hornkohl, J.O. Quantum Mechanics of the Diatomic Molecule with Applications; IOP Publishing: Bristol, UK, 2020.

[17] Parigger, C.G.; Surmick, D.M.; Helstern, C.M.; Gautam, G.; Bol'shakov, A.A; Russo, R. Molecular Laser-Induced Breakdown Spectroscopy, In Laser Induced Breakdown Spectroscopy, 2nd ed.; Singh, J.P., Thakur, S.N., Eds.; Elsevier: Amsterdam, The Netherlands, 2020; Chapter 7, pp. 167{212.

[18] Parigger, C.G. Computation of Selected Optical Transitions of Diatomic Molecules: AlO, C_2, CN, OH, N_2^+, NO, and TiO. Submitted to IRAMP, 2022.

[19] Brzozowksi, J.; Bunker, P.; Elander, N.; Erman, P. Astrophys. J. 207, 1976, 414.

[20] Erman, P. Time Resolved Spectroscopy of Small Molecules. In Molecular Spectroscopy Volume 6: A Review of the Literature published in 1977 and 1978; Barrow, R.F., Long, D.A., Sheridian, J., Eds.; The Royal Society Chemistry: London, UK, 1979; Chap. 5, 174-231.

[21] Erman P. Phys. Scr. 20, 1979, 575.

[22] Warnatz, J. Combustion Chemistry; Springer: New York, NY, USA, 1984.

[23] Raiche, G.A.; Jeries, J.B. Appl. Opt. 32, 1993, 4629.

[24] Ubachs, W.; Meijer, G.; ter Meulen, J.J.; Dymanus, A. J. Chem. Phys. 84, 1996, 3032.

[25] Parigger, C.G.; Woods, A.C.; Surmick, D.M.; Gautam, G.; Witte, M.J.; Hornkohl, J.O. Spectrochim. Acta Part B: At. Spectrosc. 107, 2015, 132.

[26] MATLAB Release R2022a Update 5 ; The MathWorks, Inc.: Natick, MA, USA, 2022.

[27] Surmick, D.M. (The University of Tennessee, University of Tennessee Space Institute, Tullahoma, TN, USA); Hornkohl, J.O. (The University of Tennessee, University of Tennessee Space Institute, Tullahoma, TN, USA). Private communication, 25 April 2016.

[28] Hornkohl, J.O. (The University of Tennessee, University of Tennessee Space Institute, Tullahoma, TN, USA). Private communication, 19 February 2004.